Original Article

Check for updates

Available online at
www.heca-analitika.com/ljes

Leuser Journal of Environmental Studies

Vol. 2, No. 2, 2024

Environmental Benefits of Palm Oil Biodiesel Enhancement: Urea Complexation Optimization via RSM

Zuchra Helwani [1,*], Said Zul Amraini [1], Sunarti Abd Rahman [2], Ida Zahrina [1], Noni Julhijah [1] and Suci Mas'ama Ulfaa [1]

[1] Department of Chemical Engineering, Universitas Riau, Pekanbaru, 28293, Indonesia; zuchra.helwani@lecturer.unri.ac.id (Z.H); saidzulamraini@lecturer.unri.ac.id (S.Z.A.); ida.zahrina@eng.unri.ac.id (I.Z); noni.julhijah0982@student.unri.ac.id (N.J); suci.masama1024@student.unri.ac.id (S.M)

[2] Faculty of Chemical and Process Engineering Technology, Universiti Malaysia Pahang Al-Sultan Abdullah, Lebuhraya Persiaran Tun Khalil Yaakob, 26300, Kuantan, Pahang, Malaysia: sunarti@umpsa.edu.my (S.A.R)

***** Correspondence: zuchra.helwani@lecturer.unri.ac.id

Article History

Received 24 July 2024
Revised 30 September 2024
Accepted 8 October 2024
Available Online 14 October 2024

Keywords:
High-performance biodiesel
Iodine number
Optimization
Urea complexation
UCF

Abstract

Indonesian commercial biodiesel often struggles with instability due to high levels of polyunsaturated fatty acids (PUFA). This study applies the urea inclusion compound (UIC) method to improve biodiesel quality by fractionating PUFA. The objective is to examine the effects of temperature, FAME/methanol ratio, and crystallization time on increasing PUFA concentration and producing high-performance biodiesel with an iodine number below 30–40 g I2/100 g. Previous studies reported a Urea Complexed Fraction (UCF) with an iodine number of 44.01 and oxidation stability of 18.61 hours at 20 °C and 4 hours crystallization. In this research, a UCF product with an iodine number of 34.18 and an 86.57% yield was achieved at 20 °C, 6 hours crystallization, and a FAME/methanol ratio of 6. The extended crystallization time and temperature significantly impacted FAME fractionation in the UCF phase. These results suggest that optimizing these process variables can enhance biodiesel stability, leading to better oxidation stability and iodine values, making the biodiesel suitable for high-performance applications in various conditions.

1. Introduction

Biodiesel, as specified by standards like ASTM D6751, IS 15607, and EN 14214, is defined as "a mixture of mono-alkyl (methyl) esters of long-chain fatty acids derived from vegetable oil or animal fat." In addition to these sources, other oleaginous materials such as microalgae, yeast-derived oils [1, 2], municipal sludge [3], and waste cooking oil [4] have also been used for biodiesel production via transesterification [5]. One of the main challenges of using raw vegetable oils or other high-lipid materials as alternative fuels in compression ignition engines is their high viscosity [6, 7]. Various techniques, including direct use and blending, microemulsion, pyrolysis, transesterification, and hydroprocessing, have been explored to address the viscosity issues associated with triglyceride-rich materials [8, 9].

Among these methods, transesterification is still the most widely used method for achieving this goal [10, 11]. To meet both the growing demand for fuel and climate change mitigation commitments, biodiesel is an appealing alternative fuel [12, 13]. Demand for biodiesel has increased over the last few decades due to policy mandates in several countries requiring biodiesel to be a part of the transportation energy mix [14, 15].

Among the many important benefits of biodiesel are its renewability, biodegradability, miscibility in diesel, cleaner emission profile, and similar fuel properties [16–18]. The feedstock's fatty acid composition significantly impacts several biodiesel properties, such as viscosity, density, cold flow characteristics, oxidative stability, cetane number, and others [19]. Due to its poor stability and poor performance at low temperatures, the fuel's widespread acceptability is limited [20, 21].

The saturated fractions of biodiesel contribute to its stability, but they can negatively affect its performance at low temperatures, particularly if they consist of long-chain saturates. At low temperatures, these long-chain saturated esters tend to crystallize due to their high melting points [22]. The cloud point (CP) is the highest temperature at which these crystals are first observed during a controlled cooling process. As the temperature drops further, the crystals continue to form and grow until the fuel reaches a point where it can no longer be pumped, known as the pour point (PP) [23]. As a result, biodiesel with a high concentration of long-chain saturated components may struggle in colder climates. To improve low-temperature performance, various strategies have been explored, such as blending with diesel or biodiesel with higher unsaturated content, adding cold-flow improvers, using alcohols with long or branched chains, and selective crystallization-fractionation (winterization) [22].

In contrast, biodiesel's unsaturation points are easily attacked, which sets off a series of oxidative reactions mediated by radicals that break down the parent molecule into various small chain compounds. Certain storage conditions, such as exposure to air, sunlight, moisture, metals, and other foreign materials, exacerbate the condition [24]. Therefore, both fatty acids—saturated and unsaturated—have benefits and drawbacks [19].

Under carefully regulated cooling conditions, winterization entails the selective crystallization of long-chain saturated components. The crystallized fractions are subsequently extracted. Selective removal of saturated fractions enriches the fuel in unsaturated mono-alkyl esters. Unsaturated fractions have a favorable effect on CFPs and viscosity, but they render the fuel susceptible to oxidative damage [19]. The fatty acid esters with multiple double bonds (polyunsaturated) are especially concerning [25]. Inadequate stability reduces the fuel's capacity for long-term storage.

The current quality of Indonesian commercial biodiesel is generally suboptimal due to the impact of certain fatty acid levels, which result in several performance drawbacks. The composition of fatty acids is a key factor in determining biodiesel quality [26, 27].. One of the limitations of biodiesel is its compatibility with petrodiesel blends, highlighting the need for quality improvements. To meet high-performance standards, Soerawidjaja [28] suggests that biodiesel should exhibit superior oxidation stability (>20 hours), a cetane number above 60, a cloud point (CP) below 5°C, and an ideal viscosity. Helwani et al. [27] proposed that one way to achieve this is by reducing polyunsaturated fatty acid (PUFA) levels through fractionation, resulting in a saturated biodiesel fraction with an iodine number of less than 30–40 g I2/100 g.

SFA and UFA are typically combined, and they need to be separated using a fractionation technique [29]. Among various methods, Schlenk & Holman [30] suggested that the urea inclusion compounds (UIC) method is a commercially viable option. This separation technique works by exploiting urea's inability to form inclusion complexes with polyunsaturated fatty acids (PUFA), allowing other fractions to be adsorbed [31]. Using this method, Bi et al. [26] successfully obtained a fraction with linolenic acid content that complies with the European Standard for Biodiesel (<12%), enhancing the efficiency of using fatty acid methyl esters (FAME) as a fuel.

Various methods for FAME fractionation have been developed, including distillation, supercritical extraction, and UIC [29, 32]. Distillation requires significant energy and can lead to material degradation due to thermal stress. Additionally, the supercritical extraction method involves high initial capital costs. Previous research has explored using AgNO3 as a solvent for biodiesel extraction to separate PUFA from SFA and MUFA, but the cost remains prohibitively high [27]. In contrast, the UIC method is more efficient, as it does not require specialized equipment and consumes less energy. This technique has proven to be the most commonly used primary fractionation method for increasing PUFA concentration [29, 33]. Furthermore, the UIC method is particularly well-suited for biodiesel production in regions with milder climates compared to tropical areas, thus enhancing the sustainability of the biodiesel production process and making it a more viable option for various environmental conditions. As biodiesel demand continues to grow globally, especially in areas with temperate climates, the use of UIC for FAME fractionation is increasingly recognized as a key process to improve fuel quality while minimizing energy costs and environmental impact.

Table 1. Levels of the fractionation variables studied in this experiment.

Variable	Coding	Unit	Levels				
			-α	-1	0	1	α
FAME/methanol ratio	X_1	% (w/v)	4	5	6	7	8
Crystallization Temp	X_2	°C	17	18	20	22	23.5
Crystallization time	X_3	hr	2.5	3	4	5	6

Note: α = 1.68

During the urea inclusion process, the urea compound, with its spiral structure, surrounds the linear hydrocarbon chains found in SFA components and some MUFA, forming a stable solid phase known as the urea-complexed fraction (UCF). However, urea struggles to form complexes with molecules that have double bonds or larger molecular structures, characteristics typically found in PUFA and some MUFA. These compounds remain in the filtrate, known as the non-urea-complexed fraction (NUCF) [29]. Several factors influence the yield and purity of each fraction when concentrating them, including the ratio of urea and alcohol solvent (C1-3) to FAME, as well as the crystallization time and temperature [33].

It is crucial to determine the optimal levels of the FAME/methanol ratio, crystallization time, and temperature in relation to the urea-to-methanol ratio and the FAME-to-urea ratio to enhance the concentration of the NUCF and UCF phases using the UIC method. To achieve this, Response Surface Methods (RSM) can be employed. The outcome would identify factor levels that result in optimal iodine values. Therefore, the objective of this research is to identify the ideal levels of the FAME/methanol ratio, crystallization time, and temperature that maximize yield and iodine number through the UIC method.

2. Materials and Methods

2.1. Materials and Tools

The materials utilized in this study included biodiesel feedstock from PT. Wilmar, urea, methanol, demineralized water, silica gel, carbon tetrachloride, potassium iodide, sodium thiosulfate, starch solution, and Wijs solution, all with a purity level of 99%. The equipment employed consisted of a glass beaker, desiccator, separating funnel, hot plate, magnetic stirrer, measuring cup, stand with clamps, a distillation setup, analytical balance, and an oven.

2.2. Solvent Extraction Stage

FAME and methanol mixtures with ratios of 1:5, 1:6, and 1:7 (v/v) were introduced into the extraction apparatus. Urea/methanol solvents with a ratio of 1:3 (w/v) were then added to the apparatus at temperatures of 18 °C, 20 °C, and 22 °C, respectively, and stirred for 3, 4, and 5 hours. After stirring, the mixture was transferred to a separating funnel and left to stand until two distinct layers formed. The upper layer, consisting of the oil phase, was separated from the lower aqueous phase, and the iodine value of the oil phase was analyzed. The bottom layer was then cooled to 15 °C to form urea crystals and an aqueous phase. The aqueous phase was separated from the urea crystals, and the iodine number was analyzed in this phase as well.

2.3. Iodine Number Analysis

The iodine number was determined following the method outlined in SNI 01-3555-1998. The sample was placed in a 500 mL Erlenmeyer flask, to which 15 mL of carbon tetrachloride and 25 mL of Wijs solution were added. The flask was sealed and kept in a dark environment for 1 to 2 hours. Afterward, 10 mL of 20% potassium iodide (KI) solution and 200 mL of distilled water were added, and the flask was shaken. Finally, 2 mL of a 0.5% (v/v) starch solution indicator was added, and the mixture was titrated using a 0.1 N sodium thiosulfate standard solution.

2.4. Gas Chromatography-Mass Spectrometry (GC-MS) Analysis

The composition of the biodiesel was analyzed using GC-MS (Shimadzu, equipped with RTX-5 MS columns with dimensions of 30 × 0.25 mm × 0.25 µm and an AOC-20i auto-injector). The samples were diluted 20-fold with hexane before being injected into the columns for analysis. In this study, we hypothesize that a second-order response surface model can be used to identify optimal points, as the characteristics of the analysis help determine the stationary point, which could represent a maximum, minimum, or saddle point in the response. To fit the second-order model, the Central Composite Design (CCD) was employed. This design allows for examining the linear, quadratic, cubic, and interaction effects of the three process variables (FAME/methanol ratio, crystallization time, and crystallization temperature) on the yield and iodine value (response) of the UCF and NUCF products obtained in the experiment. Table 1 outlines the ranges and levels of the three independent variables used in the study. The

Table 2. Fatty acid/ester composition of the initial biodiesel sample (sourced from PT. Wilmar).

No.	Component	%
1	Methyl laurate (C12:0)	0.68
2	Methyl myristate (C14:0)	2.15
3	Methyl palmitate (C16:0)	39.15
4	Methyl stearate (C18:0)	7.20
5	Methyl oleate (C18:1)	42.40
6	Methyl linoleate C18:2)	5.88
7	Others	2.54
Total		**100**

Table 3. Saturated and unsaturated fatty acid composition in the initial biodiesel sample

No.	Biodiesel feed (FAME)	%
1	Saturated FAMEs	49.18
2	Monounsaturated FAMEs	42.40
3	Polyunsaturated FAMEs	5.88
4	Others	2.54

$$X_1 = \frac{FAME/methanol\ ratio - (low + high)/2}{(high - low)/2} = \frac{\xi_1 - 6}{1} \quad (1)$$

$$X_2 = \frac{Crystallization\ Temp - (low + high)/2}{(high - low)/2} = \frac{\xi_2 - 20}{2} \quad (2)$$

$$X_3 = \frac{Crystallization\ Time - (low + high)/2}{(high - low)/2} = \frac{\xi_3 - 4}{1} \quad (3)$$

relationships between the coded and uncoded variables are illustrated in Equations 1-3.

The CCD used in this study consisted of twenty experimental points derived from three components: eight points from a two-level factorial design, six axial (or star) points, and six center points. The two-level factorial design, represented by 2^k (where $k = 3$ factors), included one minimum and one maximum level, yielding eight combinations: (-1,-1,-1), (-1,-1,1), (-1,1,-1), (-1,1,1), (1,-1,-1), (1,-1,1), (1,1,-1), and (1,1,1). The six axial points were positioned at (-α,0,0), (+α,0,0), (0,-α,0), (0,+α,0), (0,0,-α), and (0,0,+α). The six center points were located at (0,0,0). In this CCD, the alpha (α) value was set at 1.68, determined by the formula $\alpha = (nF)^{1/4}$, where nF represents the number of cube points [34].

3. Results and Discussion

3.1. GC-MS Analysis and Characterization of Biodiesel

In the fractionation stage of this research, direct processing of oils, vegetable fats, or fatty acid esters was not conducted; instead, biodiesel sourced from PT Wilmar was used as the raw material for experimentation. The fatty acid ester/acid composition of this biodiesel, as determined by GC-MS analysis, is presented in Table 2. The biodiesel sample from PT Wilmar has a cetane number of 58, a viscosity of 4.4, a density of 856.7 kg/m³, and a flash point of 158°C.

Table 3 details the composition of saturated, monounsaturated, and polyunsaturated FAME fractions based on data from GC-MS chromatograms. The iodine value of the biodiesel, measured using the Wijs method, is 57.22 g I2/100 g of sample, with an oxidation stability of 14.22 hours. This lower oxidation stability is attributed to the high concentration of PUFA in the biodiesel.

3.2. RSM Development

For each response, a mathematical model was constructed to establish the relationship between the process variables. The model incorporated first-order, second-order, and interaction effects and was expressed using a second-order polynomial equation (Equation 4):

$$Y = \beta_0 + \beta_1 X_1 + \beta_2 X_2 + \beta_3 X_3 + \beta_{11} X_{12} + \beta_{22} X_{22} + \beta_{33} X_{32} + \beta_{12} X_1 X_2 + \beta_{13} X_1 X_3 + \beta_{23} X_2 X_3 \quad (4)$$

where Y represents the predicted heating value and compressive strength, X_i and X_j represent the variables in code, b_0 is the offset term, b_i is the linear effect, b_{ij} is the first-order interaction effect, and b_{jj} is the squared effect.

Table 4 summarizes the yield and iodine number (IN) responses analyzed using the Central Composite Design (CCD) with three factors: FAME/methanol ratio (ξ_1), crystallization temperature (ξ_2), and crystallization time (ξ_3). The results for Urea Complexed Fraction (UCF) and Non-Urea Complexed Fraction (NUCF) are presented.

Table 4. Summary of various research responses to the yield (Y_1) and iodine number (Y_2).

Run	FAME/Methanol ratio(w/v)	Temp (°C)	Time (hr)	Yield (%) (Y_1)		IN (g I_2/g Biodiesel) (Y_2)	
				UCF	NUCF	UCF	NUCF
1	6	23.5	4	33.11	8.01	34.6	107.69
2	6	20	4	72.04	9.17	30.47	118.48
3	6	20	2.5	62.02	8	37.29	113.48
4	6	20	4	54.76	8.09	34.25	114.12
5	6	20	6	86.57	6.79	34.18	123.66
6	5	18	5	69.86	2.95	39.96	115.92
7	5	22	3	67.31	5.23	37.31	113.53
8	6	20	4	69.67	9.31	35.13	114.91
9	7	18	5	68.24	10.28	37.09	117.46
10	6	20	4	66.25	9.5	34.69	113.35
11	6	17	4	43.56	6.68	38.83	107.35
12	6	20	4	65.15	7.68	33.4	112.19
13	7	22	3	60.57	11.16	32.18	110.58
14	4	20	4	75.77	2.13	39.34	124.53
15	6	20	4	49.81	9.26	34.49	110.06
16	5	22	5	71.29	6.19	38.7	120.73
17	7	18	3	60	10.63	32.51	110.86
18	5	18	3	51.87	3.91	40.35	109.99
19	7	22	5	65.39	11.98	31.88	112.96
20	8	20	4	63.39	12.65	29.39	112.87

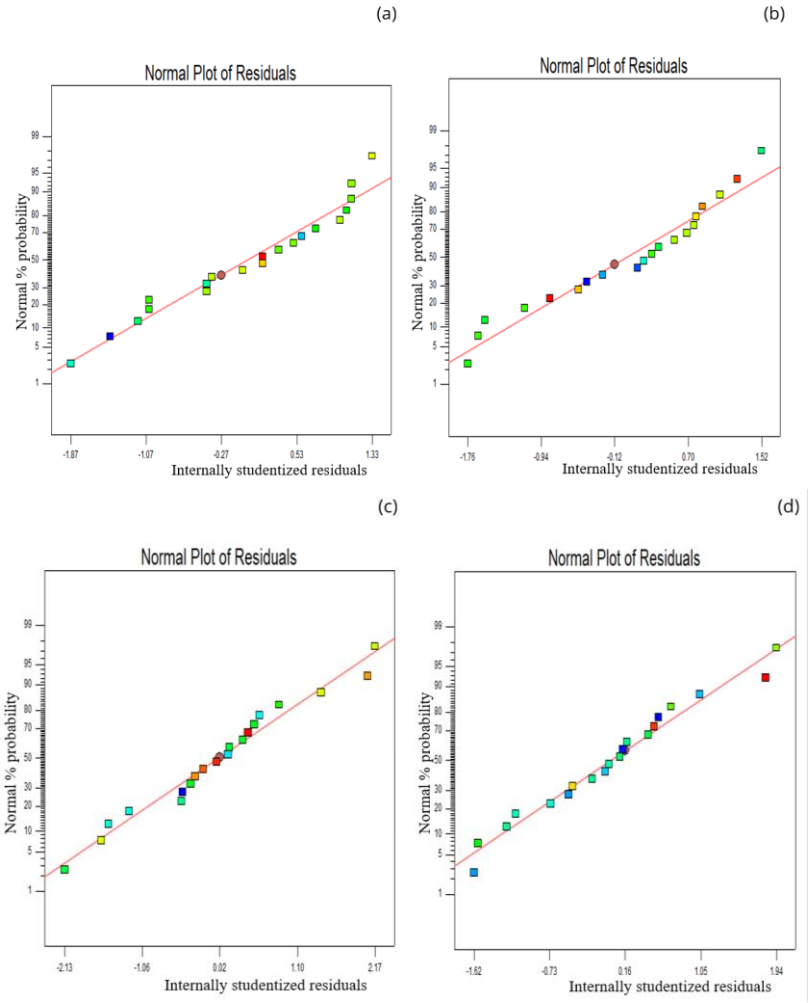

Figure 1. Normal plot versus residual (a) UCF yield (b) IN of UCF iodine (c) Yield NUCF (d) IN of NUCF.

Table 5. Statistical model summary.

	Response			
	Yield UCF	**Yield NUCF**	**IN UCF**	**IN NUCF**
Model	Quadratic	Quadratic	Quadratic	Quadratic
Sum of Squares	1527.74	6.05	21.19	165.81
Degree of freedom	9	9	9	9
Mean Square	509.25	2.02	7.06	55.27
F-value	8.81	4.02	3.60	8.24
p-value Prob >F	0.0037	0.0409	0,0537	0,0047
Standard Deviation	7.60	0.71	1.40	2.59
R^2	0.8942	0.9681	0.8900	0.8436
Adjusted R^2	0.5900	0.9394	0.7909	0.7028
Predicted R^2	0.2340	0.8688	0.2787	0.3727
Press	2052.83	20.65	128.55	268.92

Table 6. Summary of the F-Value for each response variable.

Response	**Source of variable**	**DF**	**SS**	**MS**	**F-value**	**p-value**
UCF yield	Regression	9	2101.80	0.6141	4.04	0.0201
	Error	10	578.27	57.83		
	Lack of fit	5	195.02	39.00	0.51	0.7619
	Pure error	5	383.25	76.65		
	Total	19	2680.07			
NUCF yield	Regression	9	152.41	16.93	33.74	<0.0001**
	Error	10	5.02	0.50		
	Lack of fit	5	2.17	0.43	0.76	0.6141
	Pure error	5	2.85	0.57		
	Total	19	157.43			
UCF IN	Regression	9	158.61	17.62	8.99	0.0010**
	Error	10	19.61	1.96		
	Lack of fit	5	14.88	2.98	3.15	0.1168
	Pure error	5	4.73	0.95		
	Total	19	178.22			
NUCF IN	Regression	9	361.63	40.18	5.99	0.0049**
	Error	10	67.07	6.71		
	Lack of fit	5	27.06	5.41	0.68	0.6607
	Pure error	5	40.00	8.00		
	Total	19	428.69			

The accuracy of the model can also be determined by comparing the study's actual value with predictions from the standard deviation. The model's (predicted) results were expressed as a straight line, and the research results' (actual) data were represented in the form of scattered boxes, as shown in Figure 1. This has excellent precision, so the data obtained did not have a wide spread.

Figure 1 illustrates that the data obtained shows a uniform distribution, indicating alignment between the models and the data for each response variable. The F table value was represented as F(α, df1, df2), with the probability level set at α = 0.05, where df refers to the degrees of freedom. A summary of the response curvature test results is provided in Table 5. The p-values of the model for both responses met the requirements for the p-value regression test, with p-values less than α = 0.05. These p-values were used to evaluate the influence of components on yield and iodine number variables. For both the yield and iodine number responses, the lack-of-fit p-values were insignificant (Table 6), indicating that errors resulting from model selection were not significant.

The model of UCF yield in uncoded form is presented in Equation 5:

$$UCF\ yield = 62.93 - 1.97\,A - 0.22\,B + 5.59\,C - 2.39\,A * B - 1.11\,A * C + 2.18\,B * C + 3.13A * A - 7.92\,B * B + 4.80\,C * C \quad (5)$$

For instance, using the model with a FAME-to-methanol ratio of 5, a crystallization temperature of 18 °C, and a crystallization time of 3 hours, the UCF yield is calculated to be 60%. This value is determined by the equation: 60% = 62.93 - 1.97(5) – 0.22(18 °C) + 5.59(3 hr) – 2.39(5)(18 °C) – 1.11(5)(3 hr) + 2.18(18 °C)(3 hr) + 3.13(5)(5) – 7.92(18

Table 7. p-value summary for the response of UCF and NUCF yield.

Source	*p-Value* of UCF yield	*p-Value* of NUCF yield	*p-Value* of UCF IN	*p-Value* of NUCF IN
constant	0.000*	0.000*	0.000*	0.000*
A	0.3602	<0.0001*	<0.0001*	0.0154*
B	0.9175	0.0062*	0.0083*	0.6744
C	0.0217*	0.5633	0.9925	0.0021
AB	0.3942	0.2719	0.7607	0.1033
AC	0.6874	0.8193	0.4269	0.5835
BC	0.4366	0.1541	0.4520	0.6956
A^2	0.1494	0.0553	0.5648	0.0519
B^2	0.0027	0.0478*	0.0173*	0.0049*
C^2	0.0377	0.0562	0.0854	0.0049*
R^2	0.7842	0.9681	0.8900	0.8436

Note: * means significant at α = 0.05

°C)(18 °C) + 4.80(3 hr)(3 hr). However, this 60% yield does not represent the maximum value achievable under these conditions, indicating that further optimization may be possible.

The model of the UCF Iodine Number in uncoded form is presented in Equation 6:

$$UCF\ IN = 34.05 - 2.88\,A - 1.24\,B + 0.003634\,C + 0.15\,A*B + 0.41\,A*C - 0.39\,B*C + 0.22A*A + 1.05\,B*B + 0.70C*C \quad (6)$$

For instance, using the model with a FAME-to-methanol ratio of 5, a crystallization temperature of 18 °C, and a crystallization time of 3 hours, the UCF iodine number (IN) is calculated to be 32.51 g I_2/100 g. This value is determined by the equation: 32.51 g I_2/100 g = 34.05 – 2.88(5) - 1.24(18 °C) + 0.003634(3 hr) + 0.15(5)(18 °C) + 0.41(5)(3 hr) – 0.39(18 °C)(3 hr) + 0.22(5)(5) + 1.05(18 °C)(18 °C) + 0.70(3 hr)(3 hr). However, this iodine number is not the maximum value possible, suggesting that additional optimization might yield higher values.

In the UCF yield response variable model, the main effects of C, A^2 and C^2, and the interaction effects of BC were significant (Table 7, Figures 2–4). The determination coefficient (R^2) of the UCF yield was 89.42%, which means that the model could explain UCF yield accurately because it was near 100%. For UCF IN, the main effects of C, A^2, B^2, C^2 and the interaction effect of AB and AC were significant (Table 7, Figures 6 and 7). The R^2 of compressive strength was 96.81%, which means that the NUCF yield could be largely explained by A and B through the model.

3.3. UCF Yield Analysis

Surface response graphs that show interactions between crystallization temperature (B) and crystallization time (C) with the UCF yield in FAME/methanol ratio of 5, 6, and 7, respectively, can be seen in Figure 2. At a FAME/methanol ratio of 5 and 7, the maximum UCF yield was achieved at a crystallization temperature of 22 C and a crystallization time of 3.5 hours, yielding 67.56% and 74.61%. In the meantime, the maximum UCF yield at a FAME/methanol ratio of 6 was achieved at a crystallization temperature of 20 °C and a crystallization time of 6 hours, respectively, yielding 86.57%.

Petratama & Pratama [35] state that the amount of methanol used as a solvent to dissolve urea and FAME in urea inclusion can change the solubility of urea in solution. The solubility of urea in solution will decrease with increasing solvent concentration, limiting urea's ability to incorporate saturated fatty acids. According to Jumari et al. [36], the more saturated fatty acids are absorbed in urea crystals, the longer the complexation time and the lower the complexation temperature.

Based on Figure 3, at a crystallization time of three hours, the maximum UCF yield of 60.69% was achieved at a temperature of 20 °C and a FAME/methanol ratio of six. With a FAME/methanol ratio 6 and a crystallization temperature of 20 °C, the maximum UCF yield was achieved after 4 hours of crystallization. At a FAME/methanol ratio of 7 and a crystallization temperature of 22 °C, the maximum UCF yield was achieved over a 5-hour crystallization period. According to Setyawardhani et al. [37], the solubility of inclusions between urea and fatty acids decreases with decreasing temperature, which promotes the formation of more crystals and the trapping of more saturated fatty acids in urea crystals. This will increase the concentration of saturated and some monounsaturated fatty acids in the UCF phase and increase the UCF yield.

Figure 4 visualize the influence of variable conditions on UCF yield. At a crystallization temperature of 18 °C, the highest UCF yield was obtained at 71.67% at a FAME/methanol ratio of 7 and a crystallization time of 3.5 hours. The highest UCF yield at a crystallization temperature of 20 °C with a FAME/methanol ratio of 6

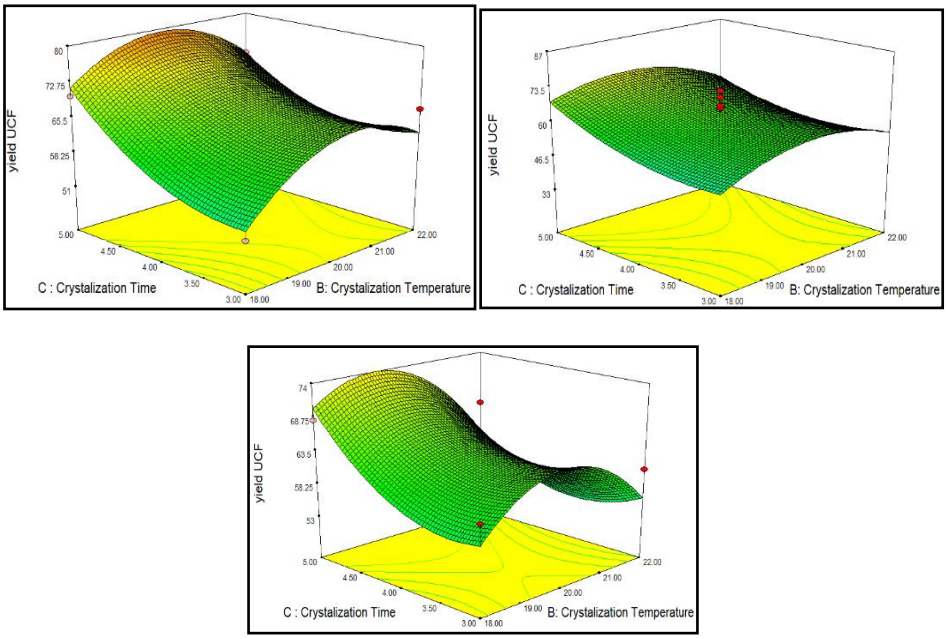

Figure 2. Graph and contour of surface response of the crystallization temperature and crystallization time effect on the UCF yield of FAME/methanol ratio (a) 5 (b) 6, and (c) 7.

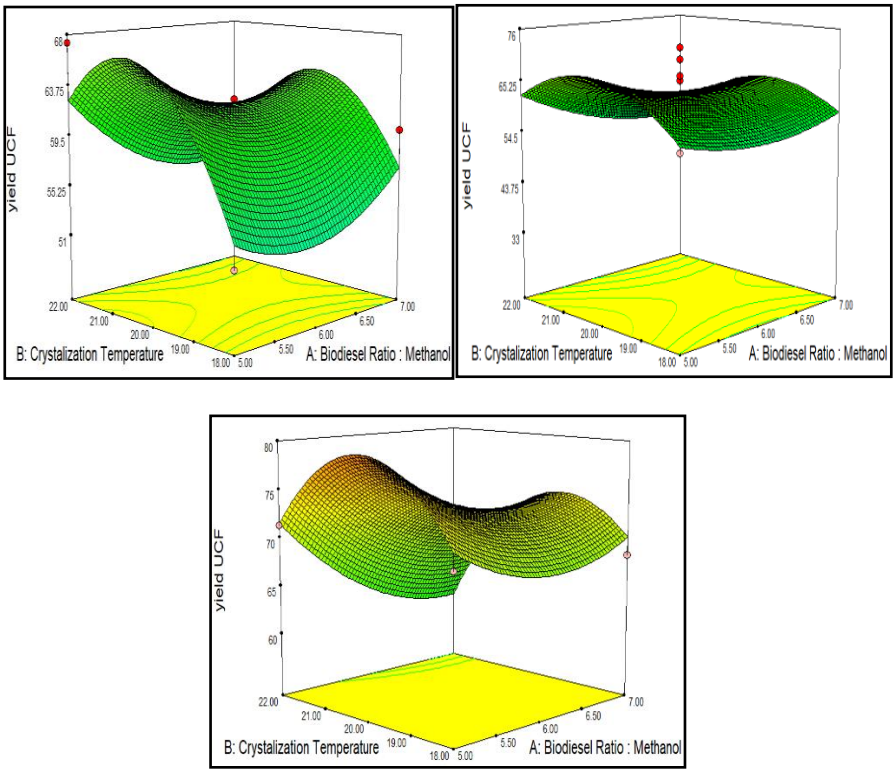

Figure 3. Graph and contour of surface response of the crystallization temperature and FAME/methanol ratio effect on the UCF yield of crystallization time, (a) 3 (b) 4, and (c) 5 hr.

And a crystallization time of 4 hours was obtained at 78.21%. Meanwhile, at a crystallization temperature of 22 °C, the highest UCF yield was obtained at 71.14% at a FAME/methanol ratio 7 and a crystallization time of 5 hours.

3.4. UFC Iodine Number Analysis

Surface response graphs that show the interactions between variable crystallization temperature (B) and crystallization time (C) with UCF IN of FAME/methanol ratio can be seen in Figure 5. The UCF iodine number at the FAME/methanol ratio of 5 was 39.879 g I_2/100 g obtained at a crystallization temperature of 22°C and a

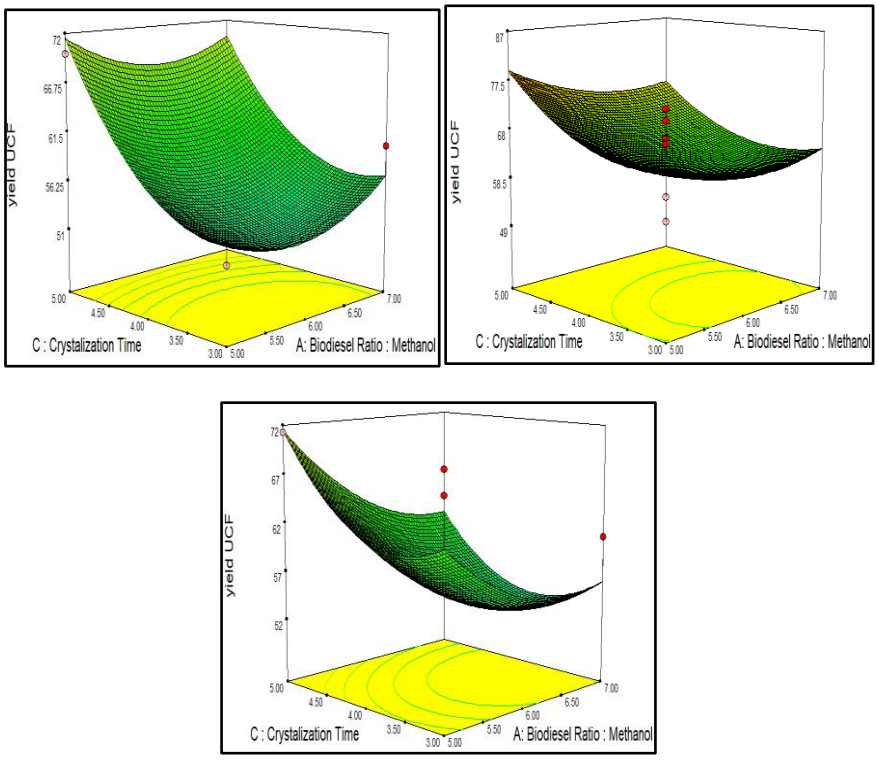

Figure 4. Graph and contour of surface response of the crystallization time and FAME:methanol ratio effect on the UCF yield of crystallization temperature (a) 18 (b) 20, and (c) 22 °C.

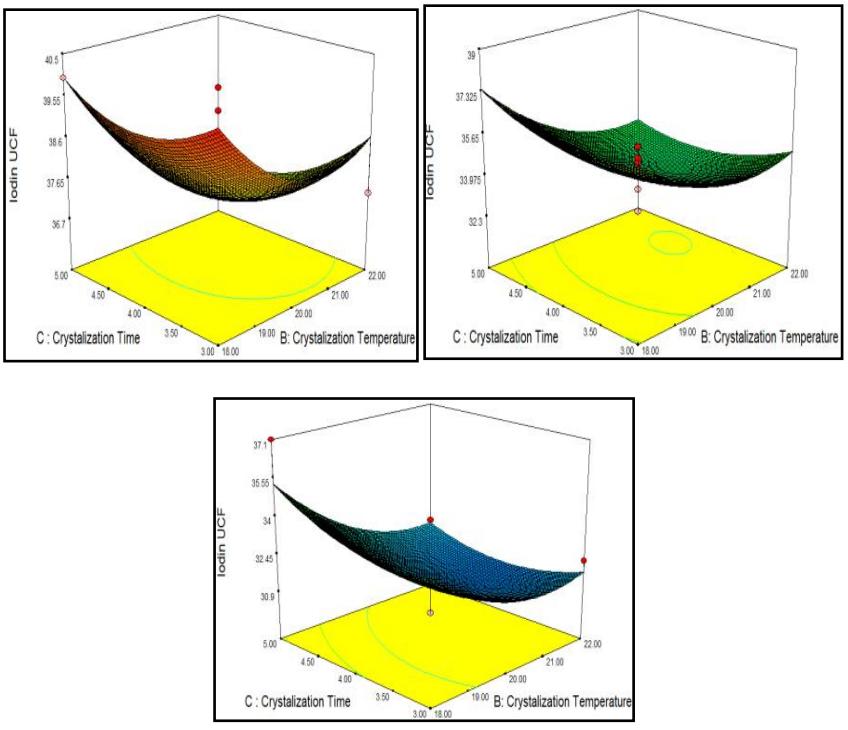

Figure 5. Graph and contour of surface response of the crystallization temperature and crystallization time effect on the UCF IN of FAME/methanol ratio (a) 5 (b) 6, and (c) 7.

crystallization time of 5 hours. The highest iodine number at the FAME/methanol ratio of 6 was 37.325 g I_2/100 g obtained at a crystallization temperature and time of 20 °C and 5 hours. When the FAME/methanol ratio was raised to 7, the UCF iodine number was recorded at 34.971 g I_2/100 g, with a crystallization time of 4.5 hours and a temperature of 22 °C.

The UCF product's iodine number will rise as the crystallization time increases. Jumari et al. [36] state that

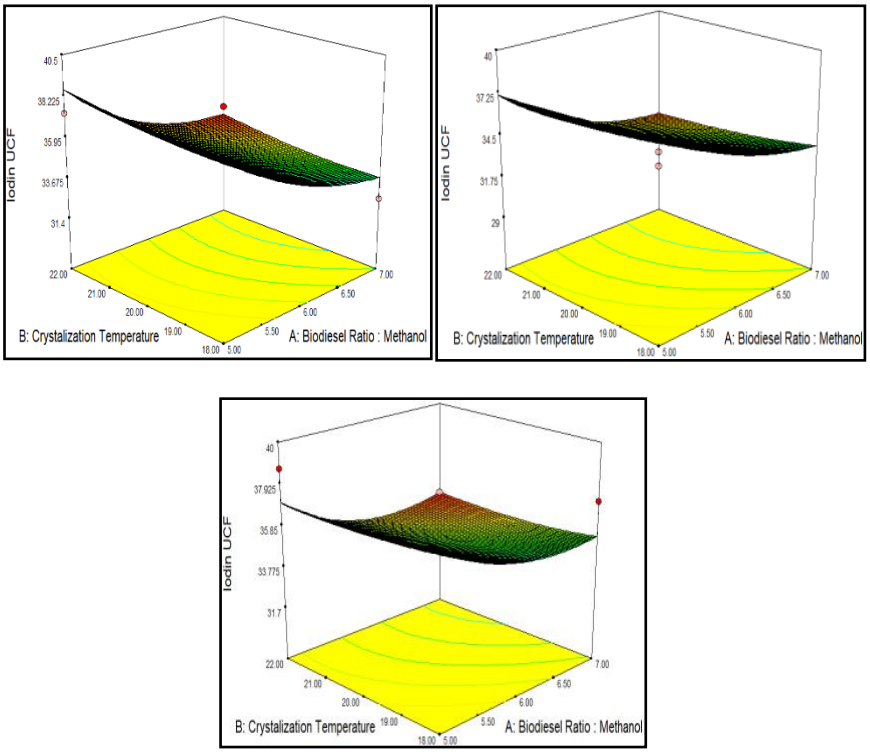

Figure 6. Graph and contour of surface response of the crystallization temperature and FAME/methanol ratio effect on the UCF IN of crystallization time, (a) 3 (b) 4, and (c) 5 hr.

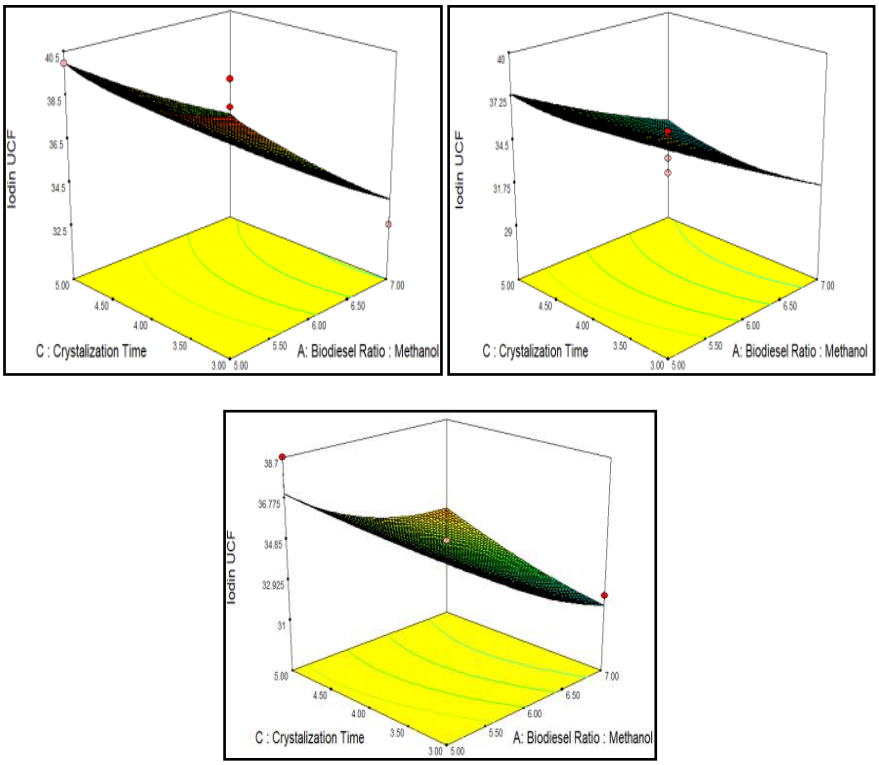

Figure 7. Graph and contour of surface response of the crystallization time and FAME/methanol ratio effect on the UCF IN of crystallization temperature (a) 18 (b) 20, and (c) 22 °C.

the Iodine number increases with a longer complexation time. This indicates that more fatty acids form complexes with urea, which increases the amount of unsaturated fatty acids in the oil. While the urea complexation process proceeds rather quickly, forming inclusions containing saturated fatty acids is slow. The oil still contains saturated fatty acids if the inclusion period is too short.

Table 8. Maximum points of yield and iodine number (IN) of UCF and NUCF products with the factor levels.

Crystallization temp (°C)	Crytallization time (hr)	FAME/ Metanol Ratio	UCF IN	UCF yield	NUCF IN	NUCF yield	Desirability
20	5	5.29	36.13	74.67	120.73	6.319	0.779
20	5	5.32	36.18	75.82	120.73	6.255	0.779
20	5	5.32	36.19	75.92	120.73	6.237	0.779
20	5	5.33	36.23	76.09	120.73	6.203	0.779

Surface response graphs that show the interactions between variable crystallization temperature (B) and FAME/methanol ratio (A) with UCF IN of crystallization time can be seen in Figure 6. The iodine number of UCF was measured at 38.454 g I_2/100 g at a FAME/methanol ratio of 7 and a crystallization temperature of 22 °C after a 3-hour crystallization period. The iodine number of UCF dropped to 37.121 g I_2/100 g after 4 hours of crystallization, with a FAME/methanol ratio of 7 and a crystallization temperature of 22 °C. The UCF product's iodine number further dropped to 36.365 g I_2/100 g at a crystallization temperature of 22 °C and a FAME/methanol ratio of 7 as the crystallization time increased to 5 hours. The iodine number of the UCF product generally decreases with increasing crystallization time; a similar decrease in iodine number is observed with increasing FAME/methanol ratio and crystallization temperature.

Surface response graphs that show interactions between crystallization time (B) and FAME/methanol ratio (C) with the UCF IN in crystallization temperatures 18, 20, and 22 ℃, respectively, can be seen in Figure 7. The highest UCF iodine number of 39.59 g I_2/100 g was obtained at a FAME/methanol ratio of 7 and a crystallization time of 4.5 hours at a temperature of 18 °C. The maximum UCF iodine number of 37.25 g I_2/100 g was obtained at a FAME/methanol ratio 6 and a crystallization time of 4 hours if the temperature was raised to 20 °C. In the meantime, with a FAME/methanol ratio of 7 and a crystallization time of 5 hours, the highest UCF iodine number dropped to 36.77 g I_2/100 g at a temperature of 22 °C. Helwani et al. [27] have identified certain requirements for high-performance biodiesel, including an iodine number in the UCF phase within 30–40 g I_2/100g. The study found that the UCF product's iodine number varied between 29.39 - 40.35 g I_2/100 g. The optimal iodine number of 30.47 g I_2/100 g was achieved at a FAME/methanol ratio 6 after 4 hours of crystallization and 20 °C crystallization temperature.

3.5. Optimization Results

The optimization results from the Design Expert 7.0 software are summarized in Table 8. The optimal UCF yield and iodine number were obtained by balancing the FAME/methanol ratio, crystallization temperature, and time. The best results were achieved at a crystallization temperature of 20 °C, crystallization time of 5 hours, and a FAME/methanol ratio of approximately 5.29. Under these conditions, the UCF yield reached 74.67%, and the iodine number was 36.13 g I_2/100 g. With a slight adjustment of the FAME/methanol ratio to 5.33, the UCF yield increased to 76.09%, and the iodine number reached 36.23 g I_2/100 g. The corresponding NUCF yield was low, approximately 6.20%, but the iodine number of the NUCF phase was significantly higher at 120.73 g I_2/100 g. The desirability score for these optimal conditions was calculated at 0.779, indicating a high level of optimization for both yield and iodine number.

4. Conclusions

The biodiesel fractionation process produced the lowest iodine number of UCF products, measuring 30.47 g I_2/100 g at a FAME/methanol ratio of 6 after 4 hours of crystallization at 20 °C. This value satisfies the requirements of high-performance biodiesel (30–40 g I_2/100 g). Concurrently, the maximum yield of UCF product (86.57%) was achieved at a FAME/methanol ratio of 6, 5.68 hours of crystallization time, and 20 °C crystallization temperature. The optimum conditions for separating saturated and polyunsaturated methyl esters from biodiesel mixtures at a FAME/methanol ratio of 5, a crystallization temperature of 20 °C and a crystallization time of 5 hours obtained a UCF yield of 74.67%, and a UCF iodine number of 36.13 g I_2/100 g. Compared to earlier studies, the iodine number obtained is more in line with the value of a high-performance biodiesel product.

Author Contributions: Conceptualization, Z.H. and I.Z..; methodology, Z.H.; software, N.J. and S.M.U.; validation, S.A.R., and Z.H.; formal analysis, I.Z..; investigation, S.Z.A.; resources, S.Z.A.; data curation, N.J. and Z.H.; writing—original draft preparation, N.J. Z.H. and S.M.U.; writing—review and editing, Z.H. and S.A.R; visualization, S.Z.A..; supervision, I.Z.; project administration, S.M.U; funding acquisition, Z.H. All authors have read and agreed to the published version of the manuscript

Funding: This research was funded by University of Riau under Mandatory Research Grant with grant number:16677/UN19.5.1.3/AL.04/2024.

Ethical Clearance: Not applicable.

Informed Consent Statement: Not applicable.

Data Availability Statement: The data supporting the findings of this study are available from the corresponding author upon reasonable request.

Conflicts of Interest: All the authors declare no conflicts of interest.

References

1. Gupta, S. K., and Dhandayuthapani, K. (2019). Microalgal Biofuels Production from Industrial and Municipal Wastewaters, *Application of Microalgae in Wastewater Treatment*, Springer International Publishing, Cham, 249–279. doi:10.1007/978-3-030-13909-4_12.
2. Ananthi, V., Siva Prakash, G., Chang, S. W., Ravindran, B., Nguyen, D. D., Vo, D.-V. N., La, D. D., Bach, Q.-V., Wong, J. W. C., Kumar Gupta, S., Selvaraj, A., and Arun, A. (2019). Enhanced Microbial Biodiesel Production from Lignocellulosic Hydrolysates Using Yeast Isolates, *Fuel*, Vol. 256, 115932. doi:10.1016/j.fuel.2019.115932.
3. Chen, J., Tyagi, R. D., Li, J., Zhang, X., Drogui, P., and Sun, F. (2018). Economic Assessment of Biodiesel Production from Wastewater Sludge, *Bioresource Technology*, Vol. 253, 41–48. doi:10.1016/j.biortech.2018.01.016.
4. Zhang, H., Aytun Ozturk, U., Wang, Q., and Zhao, Z. (2014). Biodiesel Produced by Waste Cooking Oil: Review of Recycling Modes in China, the US and Japan, *Renewable and Sustainable Energy Reviews*, Vol. 38, 677–685. doi:10.1016/j.rser.2014.07.042.
5. Sánchez, A. S., Almeida, M. B., Torres, E. A., Kalid, R. A., Cohim, E., and Gasparatos, A. (2018). Alternative Biodiesel Feedstock Systems in the Semi-arid Region of Brazil: Implications for Ecosystem Services, *Renewable and Sustainable Energy Reviews*, Vol. 81, 2744–2758. doi:10.1016/j.rser.2017.06.080.
6. Ramírez-Verduzco, L. F., Rodríguez-Rodríguez, J. E., and Jaramillo-Jacob, A. del R. (2012). Predicting Cetane Number, Kinematic Viscosity, Density and Higher Heating Value of Biodiesel from Its Fatty Acid Methyl Ester Composition, *Fuel*, Vol. 91, No. 1, 102–111. doi:10.1016/j.fuel.2011.06.070.
7. Tesfa, B., Mishra, R., Gu, F., and Powles, N. (2010). Prediction Models for Density and Viscosity of Biodiesel and Their Effects on Fuel Supply System in Ci Engines, *Renewable Energy*, Vol. 35, No. 12, 2752–2760. doi:10.1016/j.renene.2010.04.026.
8. Knothe, G. (2010). History of Vegetable Oil-Based Diesel Fuels, *The Biodiesel Handbook*, Elsevier, 5–19. doi:10.1016/B978-1-893997-62-2.50007-3.
9. Aatola, H., Larmi, M., Sarjovaara, T., and Mikkonen, S. (2009). Hydrotreated Vegetable Oil (Hvo) as a Renewable Diesel Fuel: Trade-Off between No_x, Particulate Emission, and Fuel Consumption of a Heavy Duty Engine, *SAE International Journal of Engines*, Vol. 1, No. 1, 1251–1262.
10. Guldhe, A., Singh, B., Mutanda, T., Permaul, K., and Bux, F. (2015). Advances in Synthesis of Biodiesel via Enzyme Catalysis: Novel and Sustainable Approaches, *Renewable and Sustainable Energy Reviews*, Vol. 41, 1447–1464. doi:10.1016/j.rser.2014.09.035.
11. Marwaha, A., Dhir, A., Mahla, S. K., and Mohapatra, S. K. (2018). An Overview of Solid Base Heterogeneous Catalysts for Biodiesel Production, *Catalysis Reviews*, Vol. 60, No. 4, 594–628. doi:10.1080/01614940.2018.1494782.
12. Caliskan, H. (2017). Environmental and Enviroeconomic Researches on Diesel Engines with Diesel and Biodiesel Fuels, *Journal of Cleaner Production*, Vol. 154, 125–129. doi:10.1016/j.jclepro.2017.03.168.
13. Ashok, V., Shriwastav, A., Bose, P., and Gupta, S. K. (2019). Phycoremediation of Wastewater Using Algal-Bacterial Photobioreactor: Effect of Nutrient Load and Light Intensity, *Bioresource Technology Reports*, Vol. 7, 100205. doi:10.1016/j.biteb.2019.100205.
14. Ayadi, M., Sarma, S. J., Pachapur, V. L., Brar, S. K., and Cheikh, R. Ben. (2016). History and Global Policy of Biofuels, 1–14. doi:10.1007/978-3-319-30205-8_1.
15. Souza, S. P., Seabra, J. E. A., and Nogueira, L. A. H. (2018). Feedstocks for Biodiesel Production: Brazilian and Global Perspectives, *Biofuels*, Vol. 9, No. 4, 455–478. doi:10.1080/17597269.2017.1278931.
16. Knothe, G. (2010). Biodiesel and Renewable Diesel: A Comparison, *Progress in Energy and Combustion Science*, Vol. 36, No. 3, 364–373. doi:10.1016/j.pecs.2009.11.004.
17. Helwani, Z., Amraini, S. Z., Asmura, J., Siregar, T. N., Triwahyuni, V. E., and Abd, A. A. (2023). Palm Frond Waste as a Carbon Source in the Synthesis of CaO/Biochar Catalysts for the Biodiesel Production Process, *Heca Journal of Applied Sciences*, Vol. 1, No. 1, 8–13. doi:10.60084/hjas.v1i1.9.
18. Amraini, S. Z., Sari, S., Andrio, D., Fatra, W., and Susanto, R. (2023). Optimizing Raw Material Pre-Treatment for Bioethanol Production from Empty Fruit Bunches: A Comparative Study, *Grimsa Journal of Science Engineering and Technology*, Vol. 1, No. 1, 17–23. doi:10.61975/gjset.v1i1.5.
19. Knothe, G. (2008). "Designer" Biodiesel: Optimizing Fatty Ester Composition to Improve Fuel Properties, *Energy & Fuels*, Vol. 22, No. 2, 1358–1364. doi:10.1021/ef700639e.
20. Lapuerta, M., González-García, I., Céspedes, I., Estévez, C., and Bayarri, N. (2019). Improvement of Cold Flow Properties of a New Biofuel Derived from Glycerol, *Fuel*, Vol. 242, 794–803. doi:10.1016/j.fuel.2019.01.066.
21. França, F. R. M., dos Santos Freitas, L., Ramos, A. L. D., da Silva, G. F., and Brandão, S. T. (2017). Storage and Oxidation Stability of Commercial Biodiesel Using Moringa oleifera Lam as an Antioxidant Additive, *Fuel*, Vol. 203, 627–632. doi:10.1016/j.fuel.2017.03.020.
22. Sierra-Cantor, J. F., and Guerrero-Fajardo, C. A. (2017). Methods for Improving the Cold Flow Properties of Biodiesel with High Saturated Fatty Acids Content: A Review, *Renewable and Sustainable Energy Reviews*, Vol. 72, 774–790. doi:10.1016/j.rser.2017.01.077.
23. Tyson, K. S. (2006). *Biodiesel Handling and Use Guidelines*, US Department of Energy, Energy Efficiency and Renewable Energy.
24. Liang, Y., May, C., Foon, C., Ngan, M., Hock, C., and Basiron, Y. (2006). The Effect of Natural and Synthetic Antioxidants on the Oxidative Stability of Palm Diesel, *Fuel*, Vol. 85, Nos. 5–6, 867–870. doi:10.1016/j.fuel.2005.09.003.
25. Knothe, G. (2007). Some Aspects of Biodiesel Oxidative Stability, *Fuel Processing Technology*, Vol. 88, No. 7, 669–677. doi:10.1016/j.fuproc.2007.01.005.
26. Bi, Y., Ding, D., and Wang, D. (2010). Low-Melting-Point Biodiesel Derived from Corn Oil via Urea Complexation, *Bioresource Technology*, Vol. 101, No. 4, 1220–1226. doi:10.1016/j.biortech.2009.09.036.
27. Helwani, Z., Umar, L., Neonufa, G. F., Puspawiningtyas, E., Prakoso, T., and Lugito, G. (2020). Extraction of Polyunsaturated Fatty Acids to Reduce the Iodine Number of Biodiesel Products, *IOP Conference Series: Materials Science and Engineering* (Vol. 823), IOP Publishing, 12022.
28. Soerawidjaja, T. H. (2006). Fondasi-Fondasi Ilmiah Dan Keteknikan Dari Teknologi Pembuatan Biodiesel, *Handout Seminar Nasional "Biodiesel Sebagai Energi Alternatif Masa Depan" UGM Yogyakarta*.
29. Jiang, B., Liu, Y., Zhang, L., Sun, Y., Liu, Y., and Liu, X. (2014). Study on the Concentration of Unsaturated Fatty Acid Methyl Esters by Urea Complexation., *Journal of the Chemical Society of Pakistan*, Vol. 36, No. 6.
30. Schlenk, H., and Holman, R. T. (1950). Separation and Stabilization of Fatty Acids by Urea Complexes 1, *Journal of the*

American Chemical Society, Vol. 72, No. 11, 5001–5004. doi:10.1021/ja01167a048.

31. Setyawardhani, D. A., Sulistyo, H., Sediawan, W. B., and Fahrurrozi, M. (2018). Adsorption of Saturated Fatty Acid in Urea Complexation: Kinetics and Equilibrium Studies, *AIP Conference Proceedings* (Vol. 1931), AIP Publishing LLC, 30013.
32. Guo, W., Zhu, Y., Han, Y., Luo, B., and Wei, Y. (2017). Separation Mechanism of Fatty Acids from Waste Cooking Oil and Its Flotation Performance in Iron Ore Desiliconization, *Minerals*, Vol. 7, No. 12, 244. doi:10.3390/min7120244.
33. Wanasundara, U. N. (2008). U.S Patent No. 2008/086589, Patent Cooperation Treaty.
34. Montgomery, D. C. (2019). *Introduction to Statistical Quality Control*, John Wiley & Sons, New York.
35. Petratama, F., and Pratama, A. (2018). Metode Kompleksasi Urea Sebagai Sarana Pemungutan Asam Lemak Tak Jenuh Ganda dari Minyak Goreng Sawit, *Prosiding Industrial Research Workshop and National Seminar* (Vol. 9), 144–148.
36. Jumari, A. (2015). Fraksinasi Kompleksasi Urea Pada Minyak Dedak Padi Dalam Peningkatan Konsentrasi Asam Lemak Tak Jenuh, *Ekuilibium*, Vol. 14, No. 1. doi:10.20961/ekuilibrium.v14i1.2136.
37. Setyawardhani, D. A., Sulistyo, H., Sediawan, W. B., and Fahrurrozi, M. (2015). Separating Poly-Unsaturated Fatty Acids from Vegetable Oil Using Urea Complexation: The Crystallisation Temperature Effects, *J. Eng. Sci. Technol*, Vol. 10, 41–49.